

Non-linear Regge trajectories with AdS/QCD

Miguel Angel Martin Contreras* and Alfredo Vega†

Instituto de Física y Astronomía,

Universidad de Valparaíso,

A. Gran Bretaña 1111, Valparaíso, Chile

(Dated: July 22, 2022)

In this work, we consider a non-quadratic dilaton $\Phi(z) = (\kappa z)^{2-\alpha}$ in the context of the static soft wall model to describe the mass spectrum of a wide range of vector mesons from the light up to the heavy sectors. The effect of this non-quadratic approach is translated into non-linear Regge trajectories with the generic form $M^2 = a(n+b)^\nu$. We apply this sort of fits for the isovector states of ω , ϕ , J/ψ and Υ mesons and compare with the corresponding holographic duals. We also extend these ideas to the heavy-light sector by using the isovector set of parameters to extrapolate the proper values of κ and α through the average constituent mass \bar{m} for each mesonic specie considered. In the same direction, we address the description of possible non- $q\bar{q}$ candidates using \bar{m} as a holographic threshold, associated with the structure of the exotic state, to define the values of κ and α . We study the π_1 mesons in the light sector, and the Z_c , Y and Z_b mesons in the heavy sector as possible exotic vector states. Finally, the RMS error for describing these twenty-seven states with fifteen parameters (four values for κ and α respectively and seven values for \bar{m}) is 12.61%.

I. INTRODUCTION

Nowadays, there is no doubt that hadrons are bound states of quarks and gluons, whose interactions are described by *quantum chromodynamics* (QCD). This quantum field theory is endowed with a coupling constant that controls the energy of the hadronic processes. At high energies, the smallness of the coupling constant makes the theory perturbative. On the other hand, the low energy behavior is non-perturbative. It is precisely in the latter regime where several hadronic properties are found. Also, the developed perturbative theoretical tools are insufficient to describe this particular hadronic physics. This issue motivated the development of techniques and tools that allows the direct use of QCD in the study of hadrons, such as Lattice QCD (e.g.[1]) or the use of the Dyson Schwinger equations to study hadrons (e.g.[2]).

This picture has also prompted the development of phenomenological models inspired by QCD, capturing important properties of the interaction between quarks and gluons, offering us alternatives to perform calculations of hadronic properties.

A successful example of phenomenological models for the study of hadrons is the so-called *quark potential models* [3–7], which have been remained valid since the middle seventies when the first heavy quark mesons, the J/ψ meson was observed. In this approach, the Schrödinger equation, with a potential describing the interaction between constituent heavy quarks inside the meson, provides good results describing the mesonic spectra and other properties related to the hadronic wave function, such as the decay constants [8].

From the QCD point of view, it is possible to infer the

behavior of the potential when the constituent quarks are close or far between them. In the former case, the large Q^2 limit, the coupling constant is small enough, allowing to use perturbative techniques to describe the quark interaction by considering the one-gluon exchange only. As a result, the potential is found to be Coulomb-like in this limit. On the other case, in the long-inter-quark distance, or small Q^2 limit, the strong coupling constant becomes large, preventing any perturbative machinery. In this case, quarks are considered as *confined partons*. This part of the potential cannot be explored by analytical QFT methods. But, extensive developments in *lattice QCD* proved that this term seems to be linear [9]. Similar results were found on the holographic side, where the dictionary establishes that a closed string world-sheet is dual to the Wilson loop, which accounts for confinement on the boundary theory [10–12].

Summarizing, today we know that the constituent quark interaction potential is well-motivated from QCD: it must interpolate between a Coulomb-like potential at short distances and a linear-like potential at long distances. In order to fit this phenomenological suggestion, several alternatives have been proposed (See [3–5]). The simplest realization of these sorts of ideas, giving excellent results, is just the sum of both contributions.

Another successful possibility of building phenomenological models is to study hadron properties using *gauge/gravity correspondence*. Namely the so-called bottom-up *AdS/QCD* approach allows us to calculate hadronic properties by capturing the main strong interaction features of hadrons in different mediums in an 5-dimensional AdS-like metric tensor and other background fields, as the dilaton.

In bottom-up kind of models, a dilaton field is used to induce confinement on the dual boundary theory. If

*Electronic address: miguelangel.martin@uv.cl

†Electronic address: alfredo.vega@uv.cl

Isovector meson masses (PDG)				
n	ω (MeV)	ϕ (MeV)	ψ (MeV)	Υ (MeV)
1	782.65 ± 0.12	1019.461 ± 0.016	3096.916 ± 0.011	9460.3 ± 0.26
2	$1.400 - 1450$	1698 ± 20	3686.109 ± 0.012	10023.26 ± 0.32
3	1670 ± 30	$2135 \pm 8 \pm 9$	4039 ± 1	10355 ± 0.5
4	1960 ± 25	---	4421 ± 4	10579.4 ± 1.2
5	2290 ± 20	---	---	$10889.9^{+3.2}_{-2.6}$
6	---	---	---	$10992.9^{+10.0}_{-3.1}$

Table I: This table summarises the experimental masses ([13]) for isovector mesons families consisting on ω , ϕ , ψ and Υ radial states.

the dilaton considered is static and quadratic [14], confinement is manifest by the appearance of linear Regge trajectories in the mesonic sector. Further works consider other possible forms of the dilaton field that interpolates the quadratic dilaton at high z , keeping linear trajectories (for higher quantum numbers) and allowing the study of other phenomena as chiral symmetry breaking. Linear Regge trajectories are a good description of the mesonic mass spectra in the light sector, and this has been used traditionally as a guideline in order to catch hadron properties in the AdS side of AdS / QCD models. But if hadrons contain s or heavy quarks, linearity in trajectory is lost [15–19]. For this reason, we explore other kind of dilatons in order to describe hadrons where linear Regge trajectories disagree with experimental data. This could be interesting at moment to study, for example, heavy mesons in holographic models, because as you can see in literature [20–24], AdS/QCD models applied to charmonium or bottomonium spectra are no so good enough to describe them, despite the fact that other observables (as the melting temperature) have the proper qualitative behaviour.

This work has been structured as follows: in section II we consider four families of isovector mesons with different constituent quarks and we show that these mass spectra agree with a non-linear Regge trajectory, parametrized by $M^2 = a(n+b)^\nu$. We associate the index ν with the average constituent quark mass in each case, and then we propose an expression for this index.

In section III we review holographic recipe to describe mesonic masses. We conjecture that the linearity deviation in Regge trajectories is associated, in the AdS side, with changes in the background fields, namely, the dilaton profile. We propose a dilaton deformation of the form $z^{2-\alpha}$, where α encodes the effect of the average constituent quark mass on the Regge trajectory. In section IV, we apply these ideas to the description of radial isovector states (ω , ϕ , J/ψ and Υ), with quantum numbers defined as $I^G J^{PC} = 0^-(1^{--})$.

In section V we used the isovector non-linear trajectories fitted to extrapolate the values of κ and α for K^* and the heavy-light vector mesons. We also make

a description of non- $q\bar{q}$ states by testing at the holographic level some of the proposals to describe exotic mesons as multiquark states or gluonic excitations. This exotic states can be described by considering the conformal dimension Δ associated with the operator that creates these states and how Δ affects the bulk mass term in the associated holographic potential. In this case, we use \bar{m} as a holographic threshold, defined in terms of the structure of each exotic state, to define the values of κ and α . We consider exotic candidates in the light sector (π_1 meson) as well as in the heavy one (Z_c , Z_b and X mesons).

Finally, in section VI we expose the conclusions and final comments about the present work.

II. NON-LINEAR TRAJECTORIES

The relation between hadronic squared mass and radial (and orbital) quantum number is considered usually as linear. This affirmation is in general, accepted due to experimental evidence, is especially true in the light sector, but when quark masses are increased a non-linear Regge trajectory seems better to describe hadron spectra [15–19].

In this work we consider four families of isovector mesons labeled as $I^G J^{PC} = 0^-(1^{--})$, and investigate linear and non-linear expressions for M^2 . In table I we summarize the experimental masses of all four isovector meson families considered in our analysis. In table II we show our fits for a linear and non-linear Regge trajectory expressed as

$$M_n^2 = a(n+b). \quad (1)$$

and

$$M_n^2 = a(n+b)^\nu \quad (2)$$

In Fig. 1, we summarize experimental data using both fits.

	Linear Regge Trajectory: $M^2 = a(n + b)$			Non Linear Regge Trajectory ($M^2 = a(n + b)^\nu$)			
Meson	a	b	R^2	a	b	ν	R^2
ω	1.1074	-0.3781	0.9978	1.1078	-0.3784	0.9998	0.9978
ϕ	1.7595	-0.4048	0.9999	1.8545	-0.4524	0.9617	1.000
ψ	3.2607	2.0259	0.9997	7.6516	0.4460	0.6249	0.9999
Υ	6.2015	13.9182	0.9996	85.3116	0.2849	0.1917	0.9999

Table II: Summary of linear and non linear fits for isovector meson Regge trajectories drawn in Fig. 1. We expose parameters for each parametrization considered, altogether with the correlation coefficient R^2 . Observe that linear fits bring good description of the trajectories, but R^2 decrease from unity when we increase the quark constituent mass. Also notice that the non-linear fit is more precise since R^2 is bigger than the linear one in each case.

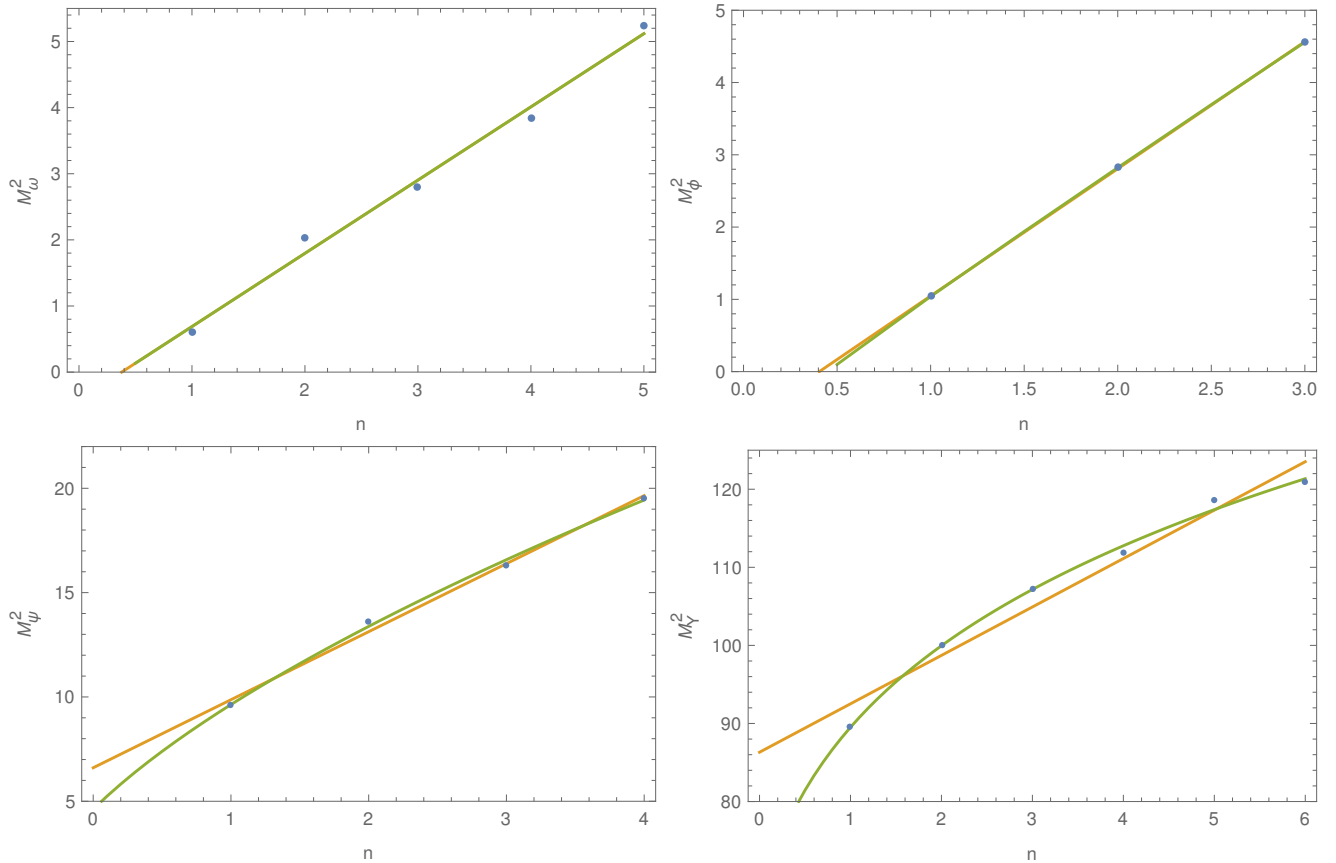


Figure 1: This plot shows M^2 vs n for different vector mesons (ω , ϕ , ψ and Υ s). Dots represent experimental data, and in each panel there are two continuous lines, one represent the best linear fit ($M^2 = a(n + b)$) and the other corresponding to a non linear fit ($M^2 = a(n + b)^\nu$).

As it is possible to see from the analysis of R^2 in table II and plot 1, the non-linear fit describe better (more accurate) the relationship between M^2 and n . Notice that the exponent ν used in the non-linear case decreases when the constituent quark mass is higher. We suggest that ν is a function of the average constituent quark masses that compose the hadron. We also propose an expression to fit the four exponents ν appearing in table II plus an additional point suggested by the chiral limit, i.e., additionally, we consider $\nu = 1$ when constituent quarks are massless.

The average constituent quark masses mentioned

above can be defined as

$$\bar{m}(q_1, q_2) = \frac{1}{2} (m_{q_1} + m_{q_2}).$$

For the constituent quark masses, we use the following set of values

$$m_u = 0.336 \text{ GeV}, \quad m_d = 0.340 \text{ GeV}, \quad m_s = 0.486 \text{ GeV}$$

$$m_c = 1.550 \text{ GeV}, \quad m_b = 4.730 \text{ GeV}$$

ω with $\alpha = 0.04$ and $\kappa = 498$ MeV				ϕ with $\alpha = 0.07$ and $\kappa = 585$ MeV			
n	M_{Exp} (MeV)	M_{Th} (MeV)	R. E. (%)	n	M_{Exp} (MeV)	M_{Th} (MeV)	R. E. (%)
1	782.65 ± 0.12	981.43	25.4	1	1019.461 ± 0.016	1139.43	11.8
2	$1400 - 1450$	1374	3.6	2	1698 ± 20	1583	5.8
3	1670 ± 30	1674	0.25	3	$2135 \pm 8 \pm 9$	1921	10
4	1960 ± 25	1967	1.7	4	Not Seen	—	—
5	2290 ± 20	2149	6.2	5	Not Seen	—	—
$M^2 = 0.9514(0.012 + n)^{0.9798}$ with $R^2 = 0.999$				$M^2 = 1.268(0.0244 + n)^{0.9650}$ with $R^2 = 0.999$			
ψ with $\alpha = 0.54$ and $\kappa = 2150$ MeV				Υ with $\alpha = 0.863$ and $\kappa = 11209$ MeV			
n	M_{Exp} (MeV)	M_{Th} (MeV)	R. E. (%)	n	M_{Exp} (MeV)	M_{Th} (MeV)	R. E. (%)
1	3096.916 ± 0.011	3077.09	0.61	1	9460.3 ± 0.26	9438.5	0.23
2	3686.109 ± 0.012	3689.62	0.1	2	10023.26 ± 0.32	9923.32	0.78
3	4039 ± 1	4137.5	2.44	3	10355 ± 0.5	10277.2	0.75
4	4421 ± 4	4499.4	1.77	4	10579.4 ± 1.2	10558.6	0.19
5	Not Seen	—	—	5	$10889.9^{+3.2}_{-2.6}$	10793.5	0.88
6	Not Seen	—	—	6	$10992.9^{+10.0}_{-3.1}$	10995.7	0.03
$M^2 = 8.07(0.287 + n)^{0.6315}$ with $R^2 = 0.999$				$M^2 = 76.511(0.901 + n)^{0.2369}$ with $R^2 = 0.999$			

Table III: Summary of results for different families of isovector radial mesonic states considered in this work. All of the mass spectra displayed in this table are calculated with the parameters mentioned on each sub-table header, using (15). The Regge trajectories are also presented in units of GeV^2 . The last column on each set of data is the relative error per state. Experimental results are read from PDG [13].

For the exponent ν introduced in the non-linear fit (2), we propose the following parameterization in terms of the average constituent quark mass given

$$\nu = a_\nu + b_\nu e^{(-c_\nu \bar{m}^2)}, \quad (3)$$

with the following model parameters

$$a_\nu = 0.1893, \quad b_\nu = 0.8221, \quad c_\nu = -0.2634.$$

Notice that in the massless constituent quark case, i.e. $\bar{m} = 0$, we recover linearity.

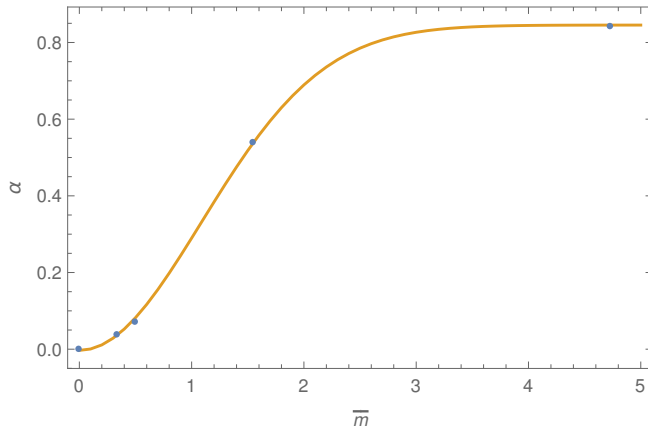


Figure 2: This plot shows the behavior of the dilaton exponent α as a function of the quark constituent mass. Notice that for low masses, dilaton should be quadratic, implying the appearance of linear Regge trajectories for such states.

III. GEOMETRIC BACKGROUND

Let us consider a five-dimensional AdS Poincar patch defined by the following metric

$$dS^2 = e^{2A(z)} [dz^2 + \eta_{\mu\nu} dx^\mu dx^\nu], \quad (4)$$

Also, we consider a bulk vector field $A_m(z, x)$ dual to isovector mesonic states interacting with a static dilaton $\Phi(z)$. This dilaton is motivated by the particle phenomenology to model confinement through the appear-

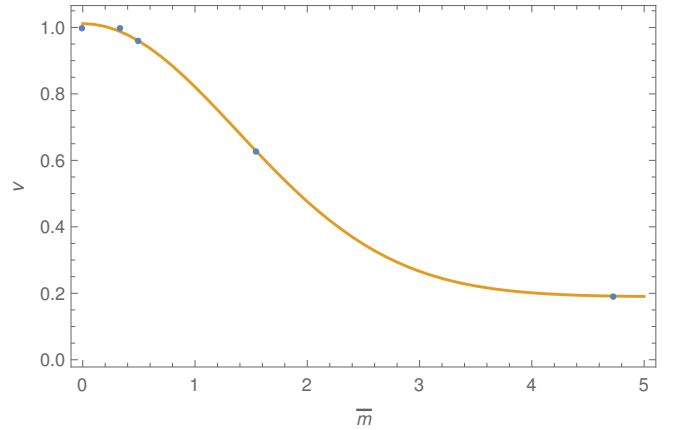


Figure 3: ν exponent as a function of the average constituent quark mass. For the massless case, it should be expected to recover $\nu = 1$.

K^* with $\alpha = 0.055$ and $\kappa = 531.24$ MeV			
n	$M_{\text{Exp}} \text{ (MeV)}$	$M_{\text{Th}} \text{ (MeV)}$	R. E. (%)
1	895.55 ± 0.8	1038.4	16.2
2	1414 ± 15	1451.0	2.6
3	1718 ± 18	1754.5	2.1

Table IV: Summary of results the vector kaon K^* radial mesonic states. The last column is the relative error per state. Experimental results are read from PDG [13].

ance of Regge trajectories. The action for such fields is

$$I_V = -\frac{1}{4g_5^2} \int d^5x \sqrt{-g} e^{-\Phi(z)} F_{mn} F^{mn}. \quad (5)$$

We have assumed the bulk vector field as massless since for mesons this quantity is fixed to be zero.

From this action, and imposing the gauge fixing $A_z = 0$, we arrive at the following equation of motion for the bulk field

$$\partial_z \left[e^{-B(z)} \partial_z A_\mu(z, q) \right] + (-q^2) e^{-B(z)} A_\mu(z, q) = 0, \quad (6)$$

where we have introduced $B(z) = \Phi(z) - A(z)$. Let us span the bulk vector field as $A_\mu(z, q) = A_\mu(q) \psi(z, q)$ in order to transform the equation of motion into a Schrödinger-like one. Performing the Bogulibov transformation $\psi(z) = e^{\Phi(z)/2} \phi(z, q)$ we arrive to the following expression

$$-\phi''(z, q) + V(z) \phi(z, q) = (-q^2) \phi(z, q) \quad (7)$$

where the holographic potential $V(z)$ is defined as

$$V(z) = \frac{1}{4} B'(z)^2 - \frac{1}{2} B''(z) \quad (8)$$

$$= \frac{3}{4z^2} + \frac{\Phi'(z)}{2z} + \frac{\Phi'(z)^2}{4} - \frac{\Phi''(z)}{2}, \quad (9)$$

where we have used the warp factor $A(z) = \log(R/z)$.

The hadronic mass spectra, and the Regge trajectories, are constructed from the eigenvalues of this potential, which is fixed by the structure of the $B(z)$ function. In the context of the original soft wall model [14], the potential is fixed by $B(z) = \kappa^2 z^2 - \log(R/z)$ obtaining the linear spectrum

$$M_n^2 = 4\kappa^2(n+1), \quad (10)$$

associated with vector mesons with massless constituent quarks. The Regge slope is identified to the κ , in units of GeV, that fixes the scale of the trajectory. The linearity observed in (10) is achieved by the specific quadratic form of the dilaton, which induces a z^2 behavior at high- z in

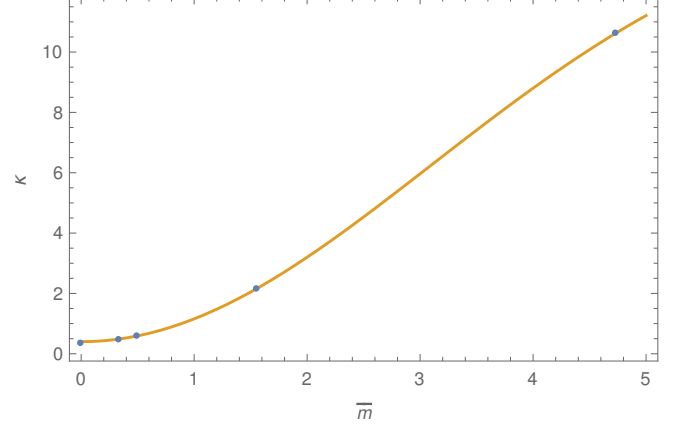


Figure 4: This plot shows how the dilaton scale κ runs with the average constituent mass. For the massless case we have used $\kappa = 0.388$ GeV [14].

the confining potential, that is translated into the linear dependence with the radial excitation number n .

If we want to consider the case when the constituent quarks are massive, we must extend to non-linear Regge trajectories [15–19]. Here we consider which this non-linearity is connected with the quark constituent mass. Therefore, massless quarks are tied to linear trajectories. Beyond the chiral symmetry breaking, once the quarks get mass, the trajectory ceases to be linear but remains as a good approximation in the light sector. A deviation in linearity in the spectrum must be associated with a change from the usual quadratic static dilaton. This deviation associated with the constituent quark mass is associated can be parametrized into a shift in the quadratic exponent of the dilaton

$$\Phi(z) = (\kappa z)^{2-\alpha}. \quad (11)$$

Fixing α to be zero, we have the massless constituent quarks. In the following sections, we will discuss the massive constituent quarks case. Exponent for dilaton (this fit consider an additional point suggested by chiral limit)

$$\alpha = a_\alpha - b_\alpha e^{(-c_\alpha \bar{m}^2)}, \quad (12)$$

with the following set of parameters:

State	$I(J^P)$	$q_1 q_2$	κ (MeV)	α	M_{Exp} (MeV)	M_{Th} (MeV)	R. E. (%)
$K^*(782)$	$1/2(1^-)$	$d \bar{s}$	531.24	0.055	895.55 ± 0.8	1038.4	16.2
$D^{*0}(2007)$	$1/2(1^-)$	$c \bar{u}$	1070.8	0.261	2006.85 ± 0.05	1902.5	5.20
$D^{*0}(2010)$	$1/2(1^-)$	$c \bar{d}$	1073.6	0.262	2010.26 ± 0.05	1906.4	5.16
D_s^{*+}	$0(?)^?$	$c \bar{s}$	1179.1	0.296	2112.2 ± 0.4	2051.7	2.86
B^{*+}	$1/2(1^-)$	$u \bar{b}$	4681.2	0.800	5324.70 ± 0.22	4561.2	14.3
B^{*0}	$1/2(1^-)$	$d \bar{b}$	4687.3	0.801	5324.70 ± 0.22	4564.4	14.27
B_s^{*0}	$0(1^-)$	$s \bar{b}$	4901.2	0.809	$5415_{-1.5}^{+1.8}$	4683.0	13.52

Table V: Summary of results for the vector heavy-light mesonic states. The last column is the relative error per state. Experimental results are read from PDG [13]. Despite the fact that D_s^{*+} has not been plenty identified, their decay modes are consistent with $J^P = 1^-$. See [13] for further details.

$$a_\alpha = 0.8454, \quad b_\alpha = 0.8485, \quad c_\alpha = 0.4233,$$

and for the energy scale κ we have the following fit

$$\kappa(\bar{m}) = a_\kappa - b_\kappa e^{-c_\kappa \bar{m}^2}, \quad (13)$$

with the following fit coefficients:

$$a_\kappa = 15.2085, \quad b_\kappa = 14.8082, \quad c_\kappa = 0.0524$$

IV. MESON MASSES

In AdS/QCD models, mesonic states are identified by the bulk field mass dual to the hadronic states in consideration. This connection is made via the conformal dimension Δ that fixes how the bulk field scales at the boundary. On the field theory side, the matching is realized by considering Δ as the scaling dimension of the operator that creates hadrons. In the case of mesons, $\Delta = 3$.

In general, from the standard AdS/CFT dictionary, we have

$$M_5^2 R^2 = (\Delta - S)(\Delta + S - 4), \quad (14)$$

where S stands for the hadron spin. In the case of isovector mesons, $\Delta = 3$ and $S = 1$ implying that such bulk vector fields are massless as we considered in the section above.

Now let us turn our attention to the holographic potential (8) constructed with the non-quadratic dilaton suggested in expression (11). This potential has the generic form

$$\begin{aligned} V_{q\bar{q}}(z, \kappa, \alpha) = & \frac{3}{4z^2} - \frac{1}{2}\alpha^2 \kappa^2 (\kappa z)^{-\alpha} + \frac{1}{4}\alpha^2 \kappa^2 (\kappa z)^{2-2\alpha} \\ & + \frac{3}{2}\alpha \kappa^2 (\kappa z)^{-\alpha} - \kappa^2 (\kappa z)^{-\alpha} - \alpha \kappa^2 (\kappa z)^{2-2\alpha} \\ & + \kappa^2 (\kappa z)^{2-2\alpha} + \frac{\kappa}{z} (\kappa z)^{1-\alpha} - \frac{\alpha \kappa}{2z} (\kappa z)^{1-\alpha}. \end{aligned} \quad (15)$$

Notice that the massless constituent quark case, when $\alpha = 0$, we recover the potential for vector mesons [14].

At this point, α becomes an extra parameter to be considered in the model. But, as we can see later, it is possible to parametrize a specific form depending on \bar{m} . This also will define a *running* for the slope κ . To properly construct these radial states, we will solve the Schrödinger equation associated with the potential (15) with α and κ as entries, for the chosen isovector family. Numerical results for each family are summarized in table III.

V. EXTRAPOLATION TO OTHER MESONIC SPECIES

Let us apply the ideas developed above to other vector mesonic systems at hand: Regge trajectory for vector kaons and masses for vector heavy-light mesons. The key idea is to use the running of α and κ with the quark constituent mass as *calibration curve* to extrapolate the proper values for other mesonic samples.

A. Kaons

Vector kaons are mesonic states labeled by $I(J^P) = 1/2(1^+)$, with $S = \pm 1$ and $C = B = 0$. In order to set the values for α and κ , we will use the following definition for the quark constituent mass as the average of the masses of s and d quarks:

$$\bar{m}_{K^*} = \frac{m_s + m_d}{2}. \quad (16)$$

With this mass, we found for the K^* system the following values for κ and α :

$$\begin{aligned} \kappa_{K^*} &= 531.24 \text{ GeV}, \\ \alpha_{K^*} &= 0.0555. \end{aligned}$$

Results for this trajectory are summarized in table IV.

B. Heavy-light mesons

Heavy-light mesons are defined as hadronic systems where one of the constituent quarks is heavy (i.e., charm or bottom) whilst the other is light flavored (up, down or strange). The physics of these heavy-light hadrons has become one of the vastest fields of research in particle physics. Calculations of the heavy-light mass spectra are done in the context of effective QFT [25], potential methods [26], QCD sum rules [27], Bethe-Salpeter equation [28] and lattice QCD [29].

Following the same procedure done in the case of vector kaons, we can fix the quark constituent mass \bar{m} as an average of the pair of constituent quarks inside the heavy-light meson. The mass spectrum and the corresponding values of κ and α are summarized in table V.

C. Non- $q\bar{q}$ vector states

All of the mesonic states with quantum numbers not allowed by the usual $q\bar{q}$ model are called *exotic*. A good review of the physics of such states can be found in [30–32] and references therein. We will focus on the vector exotic states in this section. At holographic level, [33] addresses the exotic meson spectra for Z_c and Z_b in the context of Sakai-Sugimoto models.

Holographically, as we explain above, the hadronic identity is controlled by the scaling dimension associated with the operator that creates hadrons. This information is encoded into the bulk mass of the five-dimensional field use to mimic hadrons. Equation (14) summarizes this. Therefore, if we identify the dimension of the operators that create exotic states we can address the associated vector mass spectrum by using the proper holographic potential, that in our case has the specific form

$$V_{\text{non-}q\bar{q}}(z, \kappa, \alpha, M_{5,\Delta}) = V_{q\bar{q}}(z, \kappa, \alpha) + \frac{M_5^2(\Delta) R^2}{z^2}, \quad (17)$$

where $V_{q\bar{q}}(z, \kappa, \alpha)$ is given by the expression (15). Here, we will consider the exotic meson vector states organized into two groups: *multi-quark states*. and *gluonic excitations*. The former is associated with tetraquarks, hadroquarkonium, and hadronic molecules. Pentaquarks are also part of this category. For the sake of simplicity, we will devote to multi-quark states candidates with just four constituent quarks. The methods developed here can be extrapolated to multi-quark candidates also.

At this point, it is important to mention the gauge invariance, since now we have massive bulk fields. Recall that the gauge invariance should be manifest at the conformal boundary, where all of the dual fields are massless [21]. The presence of the non-zero bulk mass does not affect the gauge $A_z = 0$. If we pay attention to the massive

e.o.m for the vector bulk fields, i.e., for the z component

$$\square A_z - \partial_z (\partial_\mu A^\mu) + M_5^2 e^{2A} A_z = 0, \quad (18)$$

and the spacetime components

$$\begin{aligned} & \partial_\nu [e^{-B} (\partial_\mu A^\mu) + \partial_z (e^{-B} A_z)] - \\ & \{ \partial_z [e^{-B} \partial_z A_\nu] + e^{-B} \square A_\nu - e^{-B} e^{-2A} M_5^2 A_\nu \} = 0, \end{aligned} \quad (19)$$

we can realize that the $A_z = 0$ gauge condition still implies $\partial_\mu A^\mu = 0$. Therefore, the fields at the boundary are still transverse.

The gluonic excitations category classifies glueballs and hybrid mesons. In this paper we will focus on vector hybrid mesons only, consisting of a quark-antiquark pair with a finite number of active gluons.

1. Multi-quark states

In the case of multi-quark states, a degeneracy appears when the conformal dimension is defined. Furthermore, since the conformal dimension is counting indirectly the number of constituent quarks, this dimension does not distinguish between four quarks in the diquark antiquark pair, the hadroquarkonium or hadronic molecule configurations.

This degeneracy can be removed if we consider the constituent mass of each multi-quark configuration as a collection of N constituents, quarks or mesons, given by

$$\bar{m}_{\text{multi-quark}} = \sum_{i=1}^N (P_i^{\text{quark}} \bar{m}_{q_i} + P_i^{\text{meson}} m_{\text{meson}_i}), \quad (20)$$

with the condition that

$$\sum_{i=1}^N (P_i^{\text{quark}} + P_i^{\text{meson}}) = 1. \quad (21)$$

Notice that each weight $P_i^{\text{quark(meson)}}$ measures the contribution of a given constituent (quark or meson) with mass $m_{\text{quark(meson)}}$. Each multi-quark state has a different mass configuration, used to calculate the parameters κ and α in the respective calibration curves, as we did in the heavy-light mesons case.

Diquark constituent model. Tetraquark states can be considered as hadronic states consisting of a pair of *diquark* and an *anti-diquark* interacting between them. A diquark is a non-colored singlet object used as essential building blocks forming tetraquark mesons and pentaquark baryons. These fundamental blocks either a color anti-triplet or a color sextet in the SU(3) color representation [34]. These diquarks are bounded by spin-spin interactions. The constituent diquark approach is

Holographic spectrum		Non- $q\bar{q}$ states		
$\Delta = 6$ and $\bar{m}_{\text{diquark-antidiquark}}$		Multiquark state		
$\alpha = 0.539$ and $\kappa = 2151$ MeV		$I^G(J^{CP}) = 1^+(1^{+-})$ Z_c mesons		
n	M_{Th} (MeV)	n	State	M_{Exp} (MeV) ΔM (%)
1	4004.8	1	$Z_c(3900)$	3887.2 ± 2.3 3.0
2	4384.9	2	$Z_c(4200)$	4196^{+35}_{-32} 4.5
3	4706.6	3	$Z_c(4430)$	4478^{+15}_{-18} 5.1
$\Delta = 6$ and $\bar{m}_{\text{hadronic molecule}}$		Multiquark state		
$\alpha = 0.539$ and $\kappa = 2151$ MeV		$I^G(J^{CP}) = 1^+(1^{+-})$ Z_c mesons		
n	M_{Th} (MeV)	n	State	M_{Exp} (MeV) ΔM (%)
1	3816.3	1	$Z_c(3900)$	3887.2 ± 2.3 1.82
2	4213.9	2	$Z_c(4200)$	4196^{+35}_{-32} 0.43
3	4551.4	3	$Z_c(4430)$	4478^{+15}_{-18} 1.64
$\Delta = 6$ and $\bar{m}_{\text{Hadrocharmonium}}$		Multiquark state		
$\alpha = 0.604$ and $\kappa = 2523$ MeV		$I^G(J^{CP}) = 0^+(1^{--})$ Y or ψ mesons		
n	M_{Th} (MeV)	n	State	M_{Exp} (MeV) ΔM (%)
1	4228.3	1	$\psi(4260)$	4230 ± 8 0.25
2	4577.3	2	$\psi(4360)$	4368 ± 13 4.8
3	4871.8	3	$\psi(4660)$	4643 ± 9 4.9
$\Delta = 6$ and $\bar{m}_{\text{Hadronic Molecule}}$		Multiquark state		
$\alpha = 0.538$ and $\kappa = 1548.7$ MeV		$I^G(J^{CP}) = 0^+(1^{--})$ Y or ψ mesons		
n	M_{Th} (MeV)	n	State	M_{Exp} (MeV) ΔM (%)
1	40027.8	1	$\psi(4260)$	4230 ± 8 5.37
2	4383.1	2	$\psi(4360)$	4368 ± 13 0.35
3	4705.1	2	$\psi(4360)$	4643 ± 9 1.34
$\Delta = 6$ and $\bar{m}_{\text{hadronic molecule}}$		Multiquark state		
$\alpha = 0.863$ and $\kappa = 11649$ MeV		$I^G(J^{CP}) = 1^+(1^{+-})$ Z_B mesons		
n	M_{Th} (MeV)	n	State	M_{Exp} (MeV) ΔM (%)
1	10410.9	1	$Z_B(10610)$	10607.2 ± 2 1.85
2	10669.3	2	$Z_B(10650)$	10652.2 ± 1.5 0.16
$\Delta = 5$ and $\bar{m}_{\text{Hybrid Meson}}$		Gluonic excitation state		
$\alpha = 0.0367$ and $\kappa = 488$ MeV		$I^G(J^{CP}) = 0^-(1^{+-})$ π_1 mesons		
n	M_{Th} (MeV)	n	State	M_{Exp} (MeV) ΔM (%)
1	1351.7	1	$\pi_1(1400)$	1354 ± 25 0.16
2	1646.6	2	$\pi_1(1600)$	1660^{+15}_{-11} 0.8
$\Delta = 5$ and $\bar{m}_{\text{Hybrid meson}}$		Gluonic Excitation		
$\alpha = 0.539$ and $\kappa = 2151$ MeV		$I^G(J^{CP}) = 1^+(1^{+-})$ Z_c mesons		
n	M_{Th} (MeV)	n	State	M_{Exp} (MeV) ΔM (%)
1	3721.9	1	$Z_c(3900)$	3887.2 ± 2.3 4.24
2	4156.4	2	$Z_c(4200)$	4196^{+35}_{-32} 0.94
3	4513.2	3	$Z_c(4430)$	4478^{+15}_{-18} 0.78
$\Delta = 7$ and $\bar{m}_{\text{Hybrid Meson}}$		Gluonic excitation state		
$\alpha = 0.863$ and $\kappa = 11649$ MeV		$I^G(J^{CP}) = 1^+(1^{+-})$ Z_B mesons		
n	M_{Th} (MeV)	n	State	M_{Exp} (MeV) ΔM (%)
1	10346.7	1	$Z_B(10610)$	10607.2 ± 2 2.52
2	10696.6	2	$Z_B(10650)$	10652.2 ± 1.5 0.42

Table VI: Summary of results for the set of non- $q\bar{q}$ states considered in this work. Experimental results are read from PDG [13].

useful to describe the spectroscopy and decays of multi-quark states. It is expected that these diquark composed candidates appear as poles in the S -matrix, described by narrow widths.

Theoretical approaches are done in the QCD sum rules [35, 36], potential models [37] framework, and lattice QCD [38], where they approach the diquark-antidiquark. Experimentally, charmonium and bottomo-

nium tetraquark states can be identified because they decay into open-flavor states instead of a quarkonium with a light meson due to the *spin-spin interaction dominance* (See [30]).

Following PDG [13], the charmonium Z_c states, with quantum numbers $I^G(J^{CP}) = 1^+(1^{+-})$, are candidates to be vector tetraquarks. For these states we can use the charm quark constituent mass given in section II to find

the values of κ and α for these states. Following Brambilla, we consider the Z_c states as a single trajectory. Table VI summarizes the experimental candidates.

Other studies, as [39], suggest $\psi(4260)$ with $0^+(1^{--})$ as a vector tetraquark instead of Z_c . As we will prove later, at least at the holographic level, $\psi(4260)$ seems to be consistent with the hypothesis that it is a hadrocharmonium state.

In this case, we can organize the diquark and antidiquark as $(q\bar{q})_1 (q\bar{q})_2$, with conformal dimension $\Delta = 6$. This implies that the bulk mass is $M_5^2 R^2 = 15$ for these states. The parameter \bar{m} can be set as a sort of *holographic threshold* that will allow us to distinguish between multi-quark state descriptions.

In the case of the diquark constituent model, the threshold in this charmonium-like diquark-antidiquark case is set as

$$\bar{m}_{\text{diquark-Antidiquark}} = \bar{m}_c, \quad (22)$$

implying that $P_i^{\text{quark}} = 1/4$ and $P_i^{\text{meson}} = 0$ for this configuration. With this definition we can set the proper values for κ and α . Numerical results for this approximation are shown in the first left panel of table VI.

Hadroquarkonium model. The hadroquarkonium states can be constructed by considering a vector meson core with a *cloud* of two quarks [40]. From the experiments, it was observed that most of the candidates to be heavy exotic states appear as final states composed by heavy quarkonium and light quarks. This motivated the idea that these states were made of a compact heavy quarkonium core surrounded by a light quark cloud [41]. This quarkonium core interacts with the light quark cloud through a *colored Van der Waals-like force* (similar as the one in molecular physics), allowing the decay of these states into the observed quarkonium core and the light quarks [42].

Following [42], we will suppose that the states $\psi(4260)$, $\psi(4360)$ and $\psi(4660)$ with $0^+(1^{--})$ are possible hadrocharmonium states, forming a single vector trajectory. Holographically, the operator that creates these states has dimension six, i.e., $\Delta = 6$, implying that the bulk mass is $M_5^2 R^2 = 15$, as in the case of the diquark-antidiquark pair configuration. The difference will be the definition of the holographic threshold used to set the parameters α and κ .

In this case, we will consider a charmonium (J/ψ meson) core characterized by its mass plus the light quark cloud, consisting of a pair of u and d quarks. Therefore, the holographic threshold is defined as

$$\bar{m}_{\text{Hadrocharmonium}} = \frac{1}{2} m_{J/\psi} + \frac{1}{4} (\bar{m}_u + \bar{m}_d). \quad (23)$$

With this criterion, we can extrapolate the model parameter and compute the mass spectra for these exotic

states. The summary of these results is shown in the third left panel of the table VI. Another possible candidates to be vector hadrocharmonium are the pair of states $\chi_{c1}(3872)$ and $\chi_{c1}(4140)$ [43], with quantum numbers given by $0^+(1^{++})$. In our case, the model developed here is not sensitive to such difference between the quantum numbers, i.e., the transition $CP = ++ \rightarrow --$ is not described by this non-quadratic dilaton (11), implying that for us these states are degenerate. A similar situation occurs in other bottom-up models, such as [44], where is not possible to distinguish between mesonic states with different isospin since the model does not consider chiral symmetry breaking. In our case, we need to add extra parameters to split up these two sets of exotic states.

Hadronic molecule model. hadronic molecules are states conformed by a pair of internal mesons bounded by strong QCD forces, interacting between them via a residual weak QCD colorless force [32]. These structures can be realized as a two heavy quarkonia interacting or one heavy quarkonium plus a light meson. This proposal is as old as QCD itself [45]. The first theoretical approaches are applications of the deuteron Weinberg's model [46, 47]. Experimental results for $X(3872)$ and $D_{S_0}(2317)$ are consistent with these ideas. Other approaches are done in the context of sum rules [48] or lattice QCD [49].

In the heavy sector, [30] and [31] suggest that Z_c or Y mesons could be possible hadronic molecule charmonium states, containing at least one pair of $c\bar{c}$ in the inner core of the molecule. The most relevant decay of these states is $J/\psi\pi$. Following this, we will construct the threshold mass for the holographic Y or ψ mesons as

$$\bar{m}_{\text{hadronic molecule}} = \frac{1}{3} m_{J/\psi} + \frac{2}{3} m_\rho. \quad (24)$$

In the case of the Z_c mesons, we have proposed the following threshold mass

$$\bar{m}_{\text{hadronic molecule}} = 0.283 m_{J/\psi} + 0.717 m_\rho. \quad (25)$$

We will extend these ideas to the bottomonium hadronic molecule candidates, the z_B mesons, where the expected core is the $\Upsilon(1S)$ state. The holographic threshold in this case is

$$\bar{m}_{\text{hadronic molecule}} = 0.458 m_{\Upsilon(1S)} + 0.542 m_\rho. \quad (26)$$

Results for all of these fits are showed in the table VI. As in the other multi-quark cases, the conformal dimension is $\Delta = 6$, implying a bulk mass given by $M^2 R^2 = 15$.

At this point, we can notice that, at the holographic level, Z_c and Y states are better described as hadronic molecules. When Z_c is described as a pair of diquark-antidiquark, the RMS error (7.5%) is bigger than in the hadronic molecule case (2.5%). For the Y mesons we observe the same: the RMS error in the hadrocharmonium

Vector hybrid meson	P_q	$P_{\bar{q}}$	P_G
π_1	0.497	0.497	6×10^{-3}
Z_c	0.49	0.49	0.02
Z_b	0.495	0.495	0.01

Table VII: Summary of coefficients fixed for each hybrid meson candidate. In the case of Z_b we are considering two flux tubes instead one.

description (6.8%) is bigger than in the molecular case (5.5%).

2. Gluonic excitations: Hybrid mesons

Gluonic excitations are defined as hadrons with constituent gluonic fields. QCD confined states are naturally non-perturbative, therefore it is not surprising to have constituent gluons inside hadrons. This kind of structure is realized as pairs of quarks and anti-quarks joined by gluonic flux tubes. This particular configuration allows us to introduce other sets of quantum numbers not possible in the quark constituent model, for example, the $J^{CP} = 1^{+-}$ configuration that we will explore in this section. The mesonic states consisting of valence quarks and constituent gluons are called *hybrid mesons*. Another set of gluonic excitations are the glueballs, not addressed here, characterized by the absence of quark quantum numbers. In general, hybrid mesons have been studied using flux tube model [50], the MIT bag model [51], coulomb-like potentials [52], gluon constituent model [53], quenched QCD [54] or lattice QCD [55].

Experimentally speaking, it is possible to find candidates across the entire mass range, from light mesons up to bottomonium states. In particular, we will focus on the π_1 , Z_c and Z_b states.

To build up the holographic description, we need to define the hadronic operators creating hybrid mesons. Following the standard AdS/QFT dictionary, the phenomenological motivation comes from the two-point functions at the conformal boundary. These objects are defined in terms of operators that are composites of quarks and gluons, that generally, can be defined as $q \gamma_\mu \bar{q} G^{\mu\nu}$, where G is a gluonic field on its ground stated and γ_μ are the Dirac matrices [56]. This, in terms of the operator dimension, means that $\Delta = 5$ if we consider one single constituent gluon, or $\Delta = 7$ if we consider two constituent gluons. This information is translated in the bulk mass as $M_5^2 R^2 = 8$ and $M_5^2 R^2 = 24$ respectively.

Since we want to define the holographic threshold, we need to infer a mass for the constituent gluon. Following [53], we adopt $M_G = 700$ MeV. Therefore, our general proposal for the holographic threshold has the form

$$\bar{m}_{\text{hybrid meson}} = P_q m_q + P_{\bar{q}} m_{\bar{q}} + P_G m_G. \quad (27)$$

In table VII we summarize the choices for the P_i coefficients used to describe the hybrid meson candidates

in the context of the model developed here. With these holographic thresholds, we can obtain the proper values for κ and α to fix the non-linear trajectory. Results are depicted in the last three panels of the table VI.

The light and the charmonium were fitted supposing a single constituent gluon, which is translated in a conformal dimension fixed as $\Delta = 6$. The RMS error in both cases is about 1% in the former and 4.4% in the latter. In the case of the bottomonium hybrids, the best fits were obtained for two constituent gluons, implying that $\Delta = 7$. The RMS error, in this case, was near to 2.55%.

It is important to notice that, at holographic level, in this model constituent gluons are not so relevant for the definition of the holographic threshold, since their associated weight in each of the three cases at hand was almost near to zero, as we can read from the table VII.

It is worthy to mention that, as a holographic prediction, the Z_c mesons are better described as a holographic hadronic molecule (R.M.S near to 2.48 %) than a holographic hybrid meson (R.M.S. near to 4.41 %).

VI. DISCUSSIONS AND CONCLUSIONS

In the model AdS/QCD with dilaton, the usual approach considers quadratic dilatons at large z , because configuration produces linear Regge trajectories. But it is important to notice that this sort of Regge trajectories is a good description only in the light sector. For this reason we propose a new shape for dilaton field, (namely $\phi(z) = (\kappa z)^{2-\alpha}$), breaking the conformal invariance and producing trajectories with the generic form $M_n^2 = a(n+b)^\nu$. This set of trajectories reproduce, in a satisfactory form, masses for vector mesons with different constituent quarks, catching linearity in the massless quark case and exhibiting how this linearity starts to cease when constituent quark masses increased.

We consider that α and ν depend on the average of constituent quark masses for the mesons considered. Also we proposed a explicit shape for $\alpha(\bar{m})$ and $\nu(\bar{m})$ in order to built a model that produce a good spectrum for vector mesons with different constituents.

Nowadays in literature, it is possible to found some models AdS/QCD applied to charmonium or bottomonium [20–24], but spectra are no so good enough in these models, although other observables (as the melting temperature) have the proper qualitative behavior. Therefore, these ideas, as we discussed here, can be useful in this kind of application.

Regarding the chiral symmetry, even though the model describes the spectra for ϕ and ω mesons, it does not reproduce a proper chiral symmetry breaking picture, as most of the static soft wall-like models developed. The main drawback is the impossibility to distinguish between the explicit and the spontaneous breaking since the quark condensate σ_q and the quark mass m_q are not independent. In the case of the dilaton proposed here, although its UV behavior is different from the static quadratic one, this does not guarantee the independence between m_q and σ_q . The best advances are done in the frame of dynamical AdS/QCD models, as [57, 58], or direct modifications of the bulk vev by changing the bulk mass, as it was done in [59].

In this direction, linear trajectories are associated with low constituent quark mass, as the results in tables II and III are demonstrating. Therefore, we conclude that the soft wall model is set before the chiral symmetry breaking scenario. Furthermore, the meson spectra obtained is degenerate: there is no form to distinguish ρ , ω and a_1 vector mesons the using quadratic dilaton only. It is necessary to do explicitly the chiral symmetry breaking by using SU(2) bulk vector fields and a tachyonic vev to address this, even though soft wall-like models do not represent a QCD-like chiral symmetry breaking. See for example the analysis done in [60].

By introducing the ν exponent in the radial Regge trajectory we can explore the effect of the quark mass. As it was pointed out in [15–17], increasing the quark mass should deviate the trajectory from the linear case. In this holographic approach, such behavior was observed. Therefore, despite the fact we do not deal with the meson structure directly, we can capture information about it in the non-linearity behavior. Translated to the bulk side, this information is captured in the α parameter, which measures the deviation from the quadratic form in the dilaton. As we observed in graphic 3, increasing constituent quark mass implies a strong deviation from the quadratic dilaton.

In the case of the energy scale κ , it is important to notice that its value is near to the constituent quark mass for each meson considered. Furthermore, in linear soft wall model, κ defines the vector Regge slope (string tension), i.e, $4\kappa^2 = a$, where the linear trajectory is defined as $M^2 = a(n + b)$. In the holographic non-linear case, where the trajectory is defined as $M^2 = a(n + b)^\nu$, the energy scale κ also increases with the quark mass, indicating that it is connected indirectly with the meson structure. In tables III, IV and V we see that each κ increases with the constituent quark mass. In the case of the non-linear trajectory, a should be proportional to κ^2 , and also carries information about the string tension and the quark constituent mass in each mesonic family. Recall that in this case, the meson is modeled as the usual

flux tube with two massive quarks at the ends, thus it is expected that the quark mass information should appear in the slope. Thus, the factor a in the non-linear trajectory should be a function of α and ν . Moreover, from the data reported in table III we can infer the fitted form for a as:

$$a(\kappa^2, \alpha, \nu) = (11.304 e^{-0.4141 \alpha} - 7.3054 e^{-0.00348 \nu}) \kappa^2, \quad (28)$$

where the correlation coefficient for this fit is $R^2 = 1$. Notice that in the case where $\alpha = 0$ (implying $\nu = 0$) and $\kappa = 388$ MeV, we obtain $a = 0.6022$ which is consistent with the usual soft wall model [14]. This expression could be useful to construct general non-linear trajectories just by using as inputs the parameters κ , α and ν .

It is worthy to say that this dilaton is not capturing the expected low z behavior in the eigenmodes. Notice that the meson ground states are not well fitted in the light sector as long as the ν exponent. This can be inferred by the fact that trajectories are not exactly fitted. Therefore, this proposed dilaton should be interpolated with other low z proposals, as [23, 61]. But, on the other hand, it was possible to fit heavy light vector mesons and to test, at holographic level, possibles candidates to be non- $q\bar{q}$ states, just by considering how the hadronic operators at the boundary change their conformal dimension, that has information about the meson constituent indirectly, altogether with the holographic threshold \bar{m} , that parameterizes the structure of the state at hand. The change in the conformal dimension is translated into a modification of the bulk mass term that appears in the holographic potential (17), whilst \bar{m} fixes in the calibration curves (13) and (12) the values for κ and α . The same methodology was used to do the holographic fit for the heavy-light mesons and the K^* vector states.

As a final comment is important to recall the precision of the holographic picture discussed in this manuscript. Although the ground states for light mesons were not well fitted (errors near to 20%), the RMS for the model with 27 mesonic states (we do not consider the non- $q\bar{q}$ states since they are holographic predictions) with 15 parameters (four values for κ and α respectively, and seven \bar{m}), we get an error near to 12.61%. Thus, this kind of non-quadratic dilaton is a strong tool to describe the holographic spectra of a wide range of mesonic species.

Acknowledgments

We wish to acknowledge the financial support provided by FONDECYT (Chile) under Grants No. 1180753 (A. V.) and No. 3180592 (M. A. M. C.).

- Phys. **33**, 477 (1994), hep-ph/9403224.
- [3] W. Lucha, F. F. Schoberl, and D. Gromes, Phys. Rept. **200**, 127 (1991).
 - [4] A. A. Bykov, I. M. Dremin, and A. V. Leonidov, Sov. Phys. Usp. **27**, 321 (1984), [Usp. Fiz. Nauk143,3(1984)].
 - [5] C. O. Dib and N. Neill, Phys. Rev. **D86**, 094011 (2012), 1208.2186.
 - [6] A. K. Rai, B. Patel, and P. C. Vinodkumar, Phys. Rev. **C78**, 055202 (2008), 0810.1832.
 - [7] B. Patel and P. C. Vinodkumar, J. Phys. **G36**, 035003 (2009), 0808.2888.
 - [8] R. Van Royen and V. F. Weisskopf, Il Nuovo Cimento A (1971-1996) **50**, 617 (1967), ISSN 1826-9869, URL <https://doi.org/10.1007/BF02823542>.
 - [9] T. Kawanai and S. Sasaki, Phys. Rev. **D92**, 094503 (2015), 1508.02178.
 - [10] O. Andreev and V. I. Zakharov, Phys. Rev. **D74**, 025023 (2006), hep-ph/0604204.
 - [11] C. D. White, Phys. Lett. **B652**, 79 (2007), hep-ph/0701157.
 - [12] F. Jugeau, Annals Phys. **325**, 1739 (2010), 0812.4903.
 - [13] M. Tanabashi et al. (Particle Data Group), Phys. Rev. **D98**, 030001 (2018).
 - [14] A. Karch, E. Katz, D. T. Son, and M. A. Stephanov, Phys. Rev. **D74**, 015005 (2006), hep-ph/0602229.
 - [15] S. S. Afonin and I. V. Pusenkov, Phys. Rev. **D90**, 094020 (2014), 1411.2390.
 - [16] J.-K. Chen, Eur. Phys. J. **C78**, 648 (2018).
 - [17] J.-K. Chen, Phys. Lett. **B786**, 477 (2018), 1807.11003.
 - [18] J.-K. Chen, Eur. Phys. J. **C78**, 235 (2018).
 - [19] S. S. Gershtein, A. K. Likhoded, and A. V. Luchinsky, Phys. Rev. **D74**, 016002 (2006), hep-ph/0602048.
 - [20] N. R. F. Braga, M. A. Martin Contreras, and S. Diles, Phys. Lett. **B763**, 203 (2016), 1507.04708.
 - [21] N. R. F. Braga, M. A. Martin Contreras, and S. Diles, EPL **115**, 31002 (2016), 1511.06373.
 - [22] N. R. F. Braga, M. A. Martin Contreras, and S. Diles, Eur. Phys. J. **C76**, 598 (2016), 1604.08296.
 - [23] N. R. F. Braga and L. F. Ferreira, Phys. Lett. **B773**, 313 (2017), 1704.05038.
 - [24] N. R. F. Braga, L. F. Ferreira, and A. Vega, Phys. Lett. **B774**, 476 (2017), 1709.05326.
 - [25] M. H. Alhakami, Phys. Rev. D **93**, 094007 (2016), 1603.08848.
 - [26] D. Ebert, R. Faustov, and V. Galkin, Eur. Phys. J. C **66**, 197 (2010), 0910.5612.
 - [27] P. Gelhausen, A. Khodjamirian, A. A. Pivovarov, and D. Rosenthal, Phys. Rev. D **88**, 014015 (2013), [Erratum: Phys.Rev.D 89, 099901 (2014), Erratum: Phys.Rev.D 91, 099901 (2015)], 1305.5432.
 - [28] L. Gutierrez-Guerrero, A. Bashir, M. A. Bedolla, and E. Santopinto, Phys. Rev. D **100**, 114032 (2019), 1911.09213.
 - [29] N. Brambilla, J. Komijani, A. Kronfeld, and A. Vairo (TUMQCD), Phys. Rev. D **97**, 034503 (2018), 1712.04983.
 - [30] N. Brambilla, S. Eidelman, C. Hanhart, A. Nefediev, C.-P. Shen, C. E. Thomas, A. Vairo, and C.-Z. Yuan (2019), 1907.07583.
 - [31] F.-K. Guo, C. Hanhart, U.-G. Meiner, Q. Wang, Q. Zhao, and B.-S. Zou, Rev. Mod. Phys. **90**, 015004 (2018), 1705.00141.
 - [32] R. F. Lebed, R. E. Mitchell, and E. S. Swanson, Prog. Part. Nucl. Phys. **93**, 143 (2017), 1610.04528.
 - [33] Y. Liu, M. A. Nowak, and I. Zahed, Phys. Rev. D **100**, 126023 (2019), URL <https://link.aps.org/doi/10.1103/PhysRevD.100.126023>.
 - [34] R. L. Jaffe, Phys. Rept. **409**, 1 (2005), [191(2004)], hep-ph/0409065.
 - [35] M. E. Bracco, S. H. Lee, M. Nielsen, and R. Rodrigues da Silva, Phys. Lett. **B671**, 240 (2009), 0807.3275.
 - [36] R. T. Kleiv, T. G. Steele, A. Zhang, and I. Blokland, Phys. Rev. **D87**, 125018 (2013), 1304.7816.
 - [37] M. Monemzadeh, N. Tazimi, and P. Sadeghi, Phys. Lett. **B741**, 124 (2015), 1507.07916.
 - [38] P. Junnarkar, N. Mathur, and M. Padmanath, Phys. Rev. **D99**, 034507 (2019), 1810.12285.
 - [39] Z.-G. Wang, Eur. Phys. J. **C78**, 933 (2018), 1809.10299.
 - [40] Y.-R. Liu, H.-X. Chen, W. Chen, X. Liu, and S.-L. Zhu, Prog. Part. Nucl. Phys. **107**, 237 (2019), 1903.11976.
 - [41] M. B. Voloshin, Prog. Part. Nucl. Phys. **61**, 455 (2008), 0711.4556.
 - [42] N. Brambilla, V. Shtabovenko, J. Tarrs Castell, and A. Vairo, Phys. Rev. **D95**, 116004 (2017), 1704.03476.
 - [43] M. Cleven, F.-K. Guo, C. Hanhart, Q. Wang, and Q. Zhao, Phys. Rev. **D92**, 014005 (2015), 1505.01771.
 - [44] E. Folco Capossoli, M. A. M. Contreras, D. Li, A. Vega, and H. Boschi-Filho (2019), 1903.06269.
 - [45] A. De Rújula, H. Georgi, and S. L. Glashow, Phys. Rev. Lett. **38**, 317 (1977), URL <https://link.aps.org/doi/10.1103/PhysRevLett.38.317>.
 - [46] S. Weinberg, Phys. Rev. **130**, 776 (1963), URL <https://link.aps.org/doi/10.1103/PhysRev.130.776>.
 - [47] J. Weinstein and N. Isgur, Phys. Rev. Lett. **48**, 659 (1982), URL <https://link.aps.org/doi/10.1103/PhysRevLett.48.659>.
 - [48] Z.-G. Wang, Z.-C. Liu, and X.-H. Zhang, Eur. Phys. J. **C64**, 373 (2009), 0907.1467.
 - [49] C. Stewart and R. Koniuk, Phys. Rev. **D57**, 5581 (1998), hep-lat/9803003.
 - [50] N. Isgur and J. E. Paton, Phys. Rev. **D31**, 2910 (1985).
 - [51] F. Iddir, A. Le Yaouanc, L. Oliver, O. Pene, J. C. Raynal, and S. Ono, Phys. Lett. **B205**, 564 (1988).
 - [52] P. Guo, A. P. Szczepaniak, G. Galata, A. Vassallo, and E. Santopinto, Phys. Rev. **D78**, 056003 (2008), 0807.2721.
 - [53] W.-S. Hou, C.-S. Luo, and G.-G. Wong, Phys. Rev. **D64**, 014028 (2001), hep-ph/0101146.
 - [54] P. Lacock, C. Michael, P. Boyle, and P. Rowland (UKQCD), Phys. Lett. **B401**, 308 (1997), hep-lat/9611011.
 - [55] J. J. Dudek, R. G. Edwards, M. J. Peardon, D. G. Richards, and C. E. Thomas (for the Hadron Spectrum Collaboration), Phys. Rev. Lett. **103**, 262001 (2009), URL <https://link.aps.org/doi/10.1103/PhysRevLett.103.262001>.
 - [56] J.-M. Richard, Few Body Syst. **57**, 1185 (2016), 1606.08593.
 - [57] T. Gherghetta, J. I. Kapusta, and T. M. Kelley, Phys. Rev. D **79**, 076003 (2009), 0902.1998.
 - [58] D. Li, M. Huang, and Q.-S. Yan, Eur. Phys. J. C **73**, 2615 (2013), 1206.2824.
 - [59] A. Vega and I. Schmidt, Phys. Rev. D **82**, 115023 (2010), 1005.3000.
 - [60] A. Ballon-Bayona and L. A. Mamani (2020), 2002.00075.
 - [61] N. R. F. Braga and L. F. Ferreira, Acta Phys. Polon. Supp. **10**, 965 (2017), 1710.07111.